Impact of Thermal Effects on Simulation Accuracy of Nonlinear Dynamics in Semiconductor Lasers

Cheng Guan Lim, *Member, IEEE*, Stavros Iezekiel, *Senior Member, IEEE*, and Christopher M. Snowden, *Fellow, IEEE*

***Abstract*—Simulations based on a carrier heating model are performed to investigate the behavior of a directly modulated 1.55-μm InGaAsP distributed feedback (DFB) laser diode (LD). Results show that bandgap shrinkage has a significant effect on the simulated nonlinear behavior of LDs. However, the varying nature of lattice temperature and excess carrier energy relaxation is important to produce simulated results that agree with measured results.**

***Index Terms*—Chaos, laser stability, nonlinear optics, semiconductor lasers.**

I. Introduction

The SEMICONDUCTOR laser diode (LD) is a device known to exhibit a rich variety of nonlinear dynamics, including chaos and self-pulsations. Such highly nonlinear behavior is normally seen as undesirable, although some applications, such as chaotic communications, rely on it. In either case, it is vital to be able to predict the nonlinear characteristics of an LD with excellent accuracy. The single-mode rate equations have been used widely [1]–[17] to simulate the large signal behavior of LDs. Over the years, the predictive power of the single-mode rate equations has been improved by the introduction of a phenomenological gain suppression factor [18]–[20]. Subsequently, the effects of current-dependent gain suppression on the accuracy of nonlinear dynamics simulation were studied [21], [22] as gain suppression had been shown to be bias-dependent [23], [24]. This dependence of the gain suppression has been attributed to the variations of lattice temperature, as optical gain is very sensitive to temperature changes. To test this postulation, the single-mode rate-equation model needs to be revised to incorporate temperature effects, which is the aim of this paper. As the effect of carrier heating dominates over lattice heating [25]–[27] for the biasing conditions considered in [21], [22], the effect of carrier heating will be specifically investigated. Hence, a carrier temperature rate equation will be presented and used in conjunction with the carrier and photon rate equations to simulate the nonlinear dynamics of a 1.55-μm distributed-feedback (DFB) LD. Calculated results will be compared to the measured results, and the research findings will be presented. To reduce any complications that might arise from inadequately accounted lattice temperature, the lattice temperature will be extracted based on the measured results.

In Section II, the carrier heating model used in this analysis and simulation considerations are presented. Simulation results are presented and discussed in Section III in three parts. In the first part, the lattice temperature is assumed to be constant for all bias currents. Here, the effects of bandgap shrinkage on simulation results will be reported. The second part is concerned with the study of longitudinal optical (LO) phonons by incorporating a LO phonon temperature rate equation. As for the final part, the varying nature of the lattice temperature is accounted for in the simulations.

Manuscript received July 7, 2004; revised December 29, 2004, and April 26, 2005.

C. G. Lim is with the Department of Photonics/Institute of Electro-Optical Engineering, National Chiao Tung University, Hsinchu 30010, Taiwan, R.O.C. (e-mail: C.G.LIM@ieee.org).

S. Iezekiel is with the School of Electronic and Electrical Engineering, University of Leeds, Leeds LS2 9JT, U.K.

C. M. Snowden is with the University of Surrey, Surrey GU2 7XH, U.K.

Digital Object Identifier 10.1109/JSTQE.2005.853748

II. Carrier Heating Model and Simulation Considerations

The first step in formulating a carrier temperature rate equation is to consider the major physical causes of carrier heating in semiconductor lasers, which are described as follows.

1) Due to the energy difference between the cladding and the active layers in semiconductor lasers, injected carriers must release this excess energy in order to relax down to the lasing band. Excess energy is redistributed to carriers in the active layer by carrier-carrier scatterings, thus causing a rise in carrier temperature.
2) Besides stimulating free carriers to recombine, photons can also be absorbed by free carriers (i.e., free-carrier absorption). This process causes the energies of absorbed photons to be transferred to free carriers, increasing their energy and hence their temperature.
3) The Auger recombination process describes the absorption of the energy released from a non-radiative carrier recombination by a free carrier, which therefore gains excess energy. Thus the carrier temperature rate equation needs to account for Auger recombination heating especially for long-wavelength LDs.
4) Spontaneous and stimulated emissions are the results of recombination of free carriers with below average energy. Therefore, the carrier reservoir in the active layer is deprived of its lowest energy carriers, causing the average carrier energy and temperature to change.
5) Finally, heated carriers relax their excess energy to longitudinal optical phonons and acoustic phonons.

1077-260X/$20.00 © 2005 IEEE

Taking these processes into account, the carrier temperature rate equation (in its general form) is formulated as

$$\frac{dT_e}{dt} = \frac{dT_{\rm inj}}{dt} + \frac{dT_{\rm fca}}{dt} + \frac{dT_{\rm Auger}}{dt} - \frac{T_e - T_L}{\tau_\epsilon} - \frac{dT_{\rm spon}}{dt} - \frac{dT_{\rm stim}}{dt} \quad (1)$$

where T_e and T_L are the average carrier temperature and lattice temperature, respectively; $T_{\rm inj}, T_{\rm fca}, T_{\rm Auger}, T_{\rm spon}$, and $T_{\rm stim}$ are the contributing temperature terms due to the injection current, free-carrier absorption, Auger recombination, spontaneous and stimulated emissions, respectively; and τ_ϵ is the carrier energy relaxation time. In a more specific form, each of the previous terms is modeled as follows. The contribution of the injection current to the average carrier temperature is given by

$$\frac{dT_{\rm inj}}{dt} = \left(\frac{\eta_i I/e}{NV}\right) E_{\rm inj} \quad (2)$$

where η_i is the internal quantum efficiency, I the injection current, e the electronic charge, N the carrier density, V the volume of the active layer, and $E_{\rm inj}$ the excess energy of an injected carrier. Free-carrier absorption heating is modeled as

$$\frac{dT_{\rm fca}}{dt} = \frac{v_g \alpha_{\rm fca} {\rm SVE}}{NV} = \frac{v_g \alpha_{\rm fca} SE}{N} \quad (3)$$

where v_g is the group velocity, $\alpha_{\rm fca}$ the free-carrier absorption coefficient, S the photon density, and E the energy of emitted photons. Auger recombination is significant in long-wavelength LDs, and its contribution to the carrier temperature is described by

$$\frac{dT_{\rm Auger}}{dt} = \left(\frac{CN^3V}{NV}\right) E_g = CN^2E_g \quad (4)$$

where C is the Auger recombination coefficient and E_g the bandgap energy. Spontaneous and stimulated emissions remove electrons from the conduction band-edge, thus reducing the population of free-electrons with the lowest energy. This affects the average carrier temperature, and their contributions can be calculated using the following:

$$\frac{dT_{\rm spon}}{dt} = \frac{T_{e(t)} - T_{e(t-\delta t)}}{\delta t} = \frac{\left(T_eNV - BN^2V\delta tE\right)/(NV) - T_e}{\delta t} = \frac{T_e - BN\delta tE - T_e}{\delta t} = -{\rm BNE} \quad (5)$$

$$\frac{dT_{\rm stim}}{dt} = \frac{T_{e(t)} - T_{e(t-\delta t)}}{\delta t} = \frac{[T_eNV - v_g{\rm GSV}\delta tE]/(NV) - T_e}{\delta t} = T_e - (v_gGS\delta tE)/N - T_e\delta t = -\frac{v_g{\rm GSE}}{N} \quad (6)$$

where B is the bimolecular recombination coefficient and G the optical gain. Gathering all contributing temperature terms and substituting them into (1) yields the following carrier heating model, which is combined with the single-mode rate equations:

$$\frac{dN}{dt} = \frac{\eta_i I}{eV} - AN - BN^2 - CN^3 - v_gGS \quad (7)$$

$$\frac{dS}{dt} = \Gamma v_gGS - \frac{S}{\tau_p} + \Gamma\beta BN^2 \quad (8)$$

$$\frac{dT_e}{dt} = \left(\frac{\eta_i I/e}{NV}\right) E_{\rm inj} + \frac{v_g\alpha_{\rm fca}SE}{N} + \frac{v_g{\rm GSE}}{N} - \frac{T_e - T_L}{\tau_\epsilon} + {\rm BNE} + CN^2E_g \quad (9)$$

where A is the nonradiative recombination coefficient, Γ the optical confinement factor, τ_p the photon lifetime, and β the spontaneous emission factor.

With reference to Fig. 1, the equation for calculating the energy of injected carriers is formulated as

$$E_{\rm inj} = E + 0.5(E_{\rm cladding} - E) \quad (10)$$

where $E_{\rm cladding}$ is the energy difference between the conduction and valence bands of the cladding, and has a value of 1.35 eV for InP cladding [29].

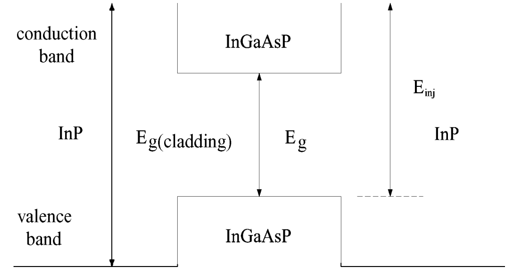

Fig. 1. Energy band diagram to demonstrate the calculation of the excess energy of an injected carrier.

The absorption $\alpha(E)$ and gain $G(E)$ models used are given by (11) [31] and (12) [32], respectively

$$\alpha(E) = \left(\frac{e^2h|M_b|^2}{4\pi^2\epsilon_o m_o^2 cnE}\right) \times \left(\frac{2m_r}{\hbar^2}\right)^{3/2} \times (E - E_g)^{1/2} \times [1 - f_c(E_c) - f_v(E_v)] \quad (11)$$

$$G(E) = \left(\frac{e^2h|M_b|^2}{4\pi^2\epsilon_o m_o^2 cnE}\right) \times \left(\frac{2m_r}{\hbar^2}\right)^{3/2} \times (E - E_g)^{1/2} \times f_c(E_c) \times f_v(E_v) \quad (12)$$

where h is Planck's constant, $\hbar$ the reduced Planck's constant, n the refractive index of the active layer, c the speed of light in vacuum, ϵ_o the permittivity of free-space, m_o the free-electron mass, m_r a mass ratio, $|M_b|^2$ the average matrix element for the Bloch states, $f_c(E_c)$ the occupation probability of an electron

with the energy E_c, and $f_v(E_v)$ is the occupation probability of a hole with the energy E_v.

Change in refractive index (δn) of the active layer due to carrier density change (δn_N) and current-induced heating (δn_T) is calculated as follows:

$$\delta n = \delta n_N + \delta n_T = \delta N \left(\frac{\partial n}{\partial N}\right) + \left(\frac{1}{2\Lambda}\right) \delta T \left(\frac{\partial \lambda}{\partial T}\right) \tag{13}$$

where δN is the change in carrier density, dn/dN the rate of change in refractive index with carrier density, Λ the corrugation periodicity, δT the temperature change and $d\lambda/dT$ the rate of change in emission wavelength with temperature.

As the refractive index changes, there is a corresponding shift in lasing wavelength

$$\delta \lambda = \delta \lambda_N + \delta \lambda_T = (2\Lambda)\delta N \left(\frac{\partial n}{\partial N}\right) + \delta T \left(\frac{\partial \lambda}{\partial T}\right) \tag{14}$$

where $\delta\lambda$ is the overall wavelength-shift, $\delta\lambda_N$ the carrier-induced wavelength-shift, and $\delta\lambda_T$ the wavelength shift caused by current-induced heating.

Besides bandgap shrinkage, the index change due to variations in carrier density and current-induced heating, and subsequent blue-shifting and red-shifting of the operating wavelength, are also taken into account by varying the photon energy. The optical absorption and gain experienced by the shifted operating wavelength are calculated using (11) and (12), respectively, with the corresponding value of $|M_b|^2, n, E, E_g, f_c(E_c)$, and $f_v(E_v)$ at each shifted operating wavelength. Finally, the change in group velocity due to refractive index change is also considered.

All these changes are accounted for in the simulations through the change in all n- and E-related terms in (7)–(14). The magnitude of E is obtained from

$$E = h\left(\frac{c}{\lambda + \delta\lambda}\right) + \delta T \left(\frac{dE}{dT}\right) \tag{15}$$

where λ is the lasing wavelength.

III. Results and Discussions

In this section, the nonlinear dynamics of a directly modulated 1.55-μm DFB LD having the parameters shown in Table I will be studied numerically. In the first part of this analysis, T_L was assumed to be constant, under all biasing conditions, and τ_ϵ was assumed to be fixed at the value determined by the bias current and does not vary with modulation conditions.

As can be observed from the femtosecond pump-probe transmission measurement performed in [33] for a semiconductor optical device having very similar characteristics with the device in this work, carriers lose their excess energy in three phases (i.e., ultrafast, fast, and slow). By neglecting the long energy relaxation process, the value of τ_ϵ at threshold was estimated to be 1.333 ps. With this value, T_L was found to be 339 K at threshold by fitting the calculated L–I curve to measured results. For the first case, T_L will be assumed to be at this value for other bias

TABLE I
Parameter Values of a 1.55 μm InGaAsP Distributed Feedback (DFB) Semiconductor Laser

Parameter (Symbol)	Value
Composition of Gallium (x)	0.411
Composition of Arsenide (y)	0.884
Avg. matrix element, Bloch states ($\lvert M_b\rvert^2$)	2.379×10^{-49} Jg
Mass ratio (m_r)	3.758×10^{-32}
Conduction band mass (m_c)	4.147×10^{-32} g
Heavy hole mass (m_{hh})	4.01×10^{-31} g
Light hole mass (m_{lh})	5.304×10^{-32} g
Spin-orbit coupling (Δ)	5.026×10^{-20} J
Bandgap energy (E_g)	1.293×10^{-19} J
Corrugation periodicity (Λ)	240 nm
Refractive index (n)	3.552
Group velocity (v_g)	8.44×10^{7} ms^{-1}
Internal quantum efficiency (η_i)	1 [14]
Volume of active layer (V)	6.75×10^{-17} m^3 [14]
Photon lifetime (τ_p)	1.75 ps [14]
Optical confinement factor (Γ)	0.35 [14]
Nonradiative recombination coefficient (A)	10^8 s^{-1} [14]
Bimolecular recombination coefficient (B)	1.25×10^{-16} m^{3}s^{-1} [14]
Auger recombination coefficient (C)	3.5×10^{-41} m^{6}s^{-1} [14]
Spontaneous emission factor (β)	8×10^{-7} [14]
Bandgap shrinkage rate	0.325 meV/K [28]
Free-carrier absorption rate ($v_g\alpha_{fca}$)	2.815×10^{3} s^{-1} [29]
Carrier-induced index-change	-1.8×10^{-26} m^3 [30]
Current-induced heating wavelength-shift	0.09 nm/$^\circ$C [31]

currents. From the bifurcation maps shown in Fig. 2, it was noted that the simulated results do not resemble the measured results at all. This is due to neglecting the bandgap shrinkage effect [a phenomenon that has an adverse effect on the gain spectrum (Fig. 3)] as can be seen from the behavioral maps (Fig. 4) obtained from simulations that accounted for bandgap shrinkage. In the latter case, the value of T_L at threshold was found to be 447 K, and the simulated behavioral maps are very similar to those simulated using constant gain suppression [21], [22]. However, discrepencies arise when comparing them with the measured results [14].

In the second part of the investigation, simulations were based on a two-level carrier heating model by incoporating a longitudinal optical phonon temperature rate equation shown in (16), and changing T_L as in (9) to the LO phonon temperature (i.e., $T_{\rm LO}$)

$$\frac{dT_{\rm LO}}{dt} = \frac{T_e - T_{\rm LO}}{\tau_\epsilon} - \frac{T_{\rm LO} - T_L}{\tau_{\rm LO}} \tag{16}$$

where $T_{\rm LO}$ is the longitudinal optical phonon temperature, and $\tau_{\rm LO}$ is the longitudinal optical phonon lifetime.

Hall *et al.* [33] have suggested that heat carrier distribution cools to an equilibrium temperature with a time constant of approximately 1 ps. As mentioned earlier, carriers lose their excess energy in three phases (i.e., ultrafast, fast, and slow phases). The estimated values for τ_ϵ by considering only the ultrafast decay phase are 0.733, 0.556, and 0.467 ps in the absorption, transparency, and gain regions, respectively. These values give an average value of 0.585 ps. However, if the fast energy decaying phase is also taken into account together with the ultrafast energy decaying phase to estimate the value of τ_ϵ, then the estimated values in the absorption, transparency, and gain regions

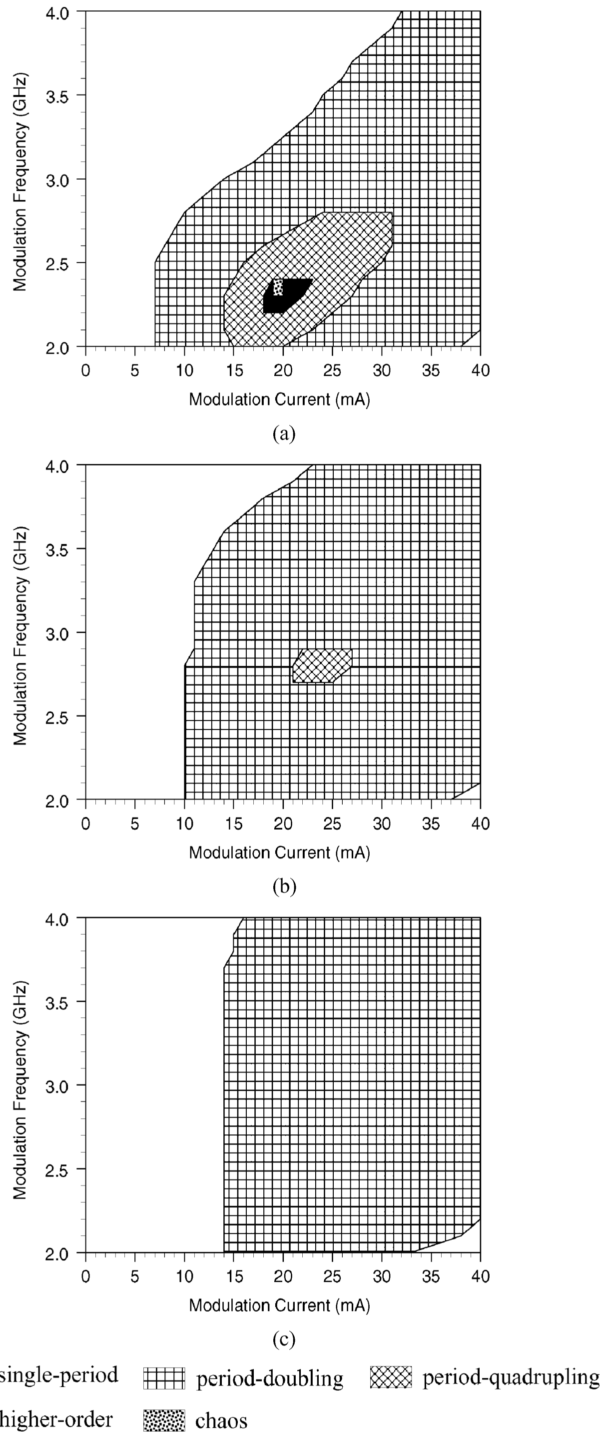

Fig. 2. Bifurcation regions considering a lattice temperature of 339 K and without taking bandgap shrinkage and carrier-induced index change into account. (a) $I_{\mathrm{dc}} = 18$ mA. (b) $I_{\mathrm{dc}} = 20$ mA. (c) $I_{\mathrm{dc}} = 22$ mA.

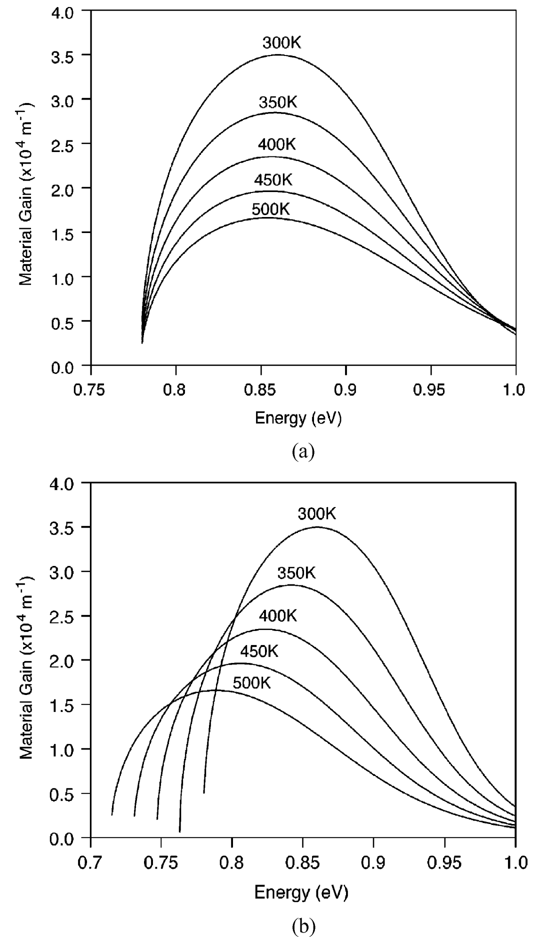

Fig. 3. Calculated gain spectra of the DFB LD at the threshold carrier density (i.e., 2.32×10^{24} m^{-3}). (a) Bandgap shrinkage was not taken into consideration. (b) Bandgap shrinkage was accounted for.

are 1.4, 1.422 and 1.111 ps, respectively. These values give a mean value of 1.311 ps for τ_ϵ. In the simulations that follow, a value of 0.948 ps (i.e., the average of the above two mean values) is used for τ_ϵ. Simulated results showed that by taking T_L to be constant at 300 K, the carrier heating effect on the nonlinear dynamics of laser diode cannot be observed because of the relatively much shorter τ_ϵ as compared to the modulation period. In other words, T_e would have relaxed to 300 K on a time scale that is much shorter than one modulation period; hence, after the carrier energy relaxation phase, there is no sign of gain suppression. This deduces the same conclusion made before that T_L does not stay constant at 300 K. Instead it varies with the bias current.

A reverse engineering approach was used, whereby simulated results were fitted to measured results by varying T_L and τ_{LO} at each of the selected modulation frequencies for each of the bias currents. Fitting begins by assuming the appropriate extracted value of τ_{LO} for the bias current considered, and varying T_L. The optical gain calculated here (approximately 2×10^4 m^{-1}) is the same as that calculated using the conventional single-mode rate equation model that uses differential gain [32]. With the aid of the calculated gain spectra of this LD [Fig. 3(b)], T_L was estimated to be around 450 K. If no acceptable results were obtained, T_L was varied and τ_{LO} was changed accordingly. This process was repeated until the values of T_L and τ_{LO} that yield the best-fitted calculated nonlinear behavior were obtained. For this case, the best choice of T_L and τ_{LO} at each selected modulation frequency (i.e., 2.0, 2.5, 3.0, 3.5, and 4.0 GHz) is shown in Fig. 5(a) and

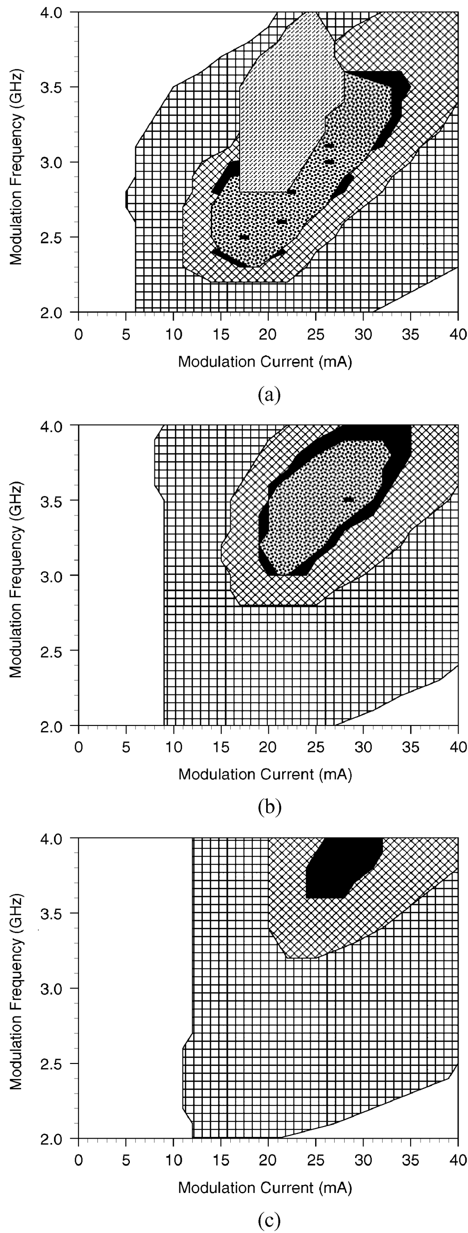

Fig. 4. Route of bifurcation for the case where T_L is 447 K and effects of bandgap shrinkage and refractive index change due to variation of carrier density are taken into account. (a) $I_{\mathrm{dc}} = 18$ mA. (b) $I_{\mathrm{dc}} = 20$ mA. (c) $I_{\mathrm{dc}} = 22$ mA.

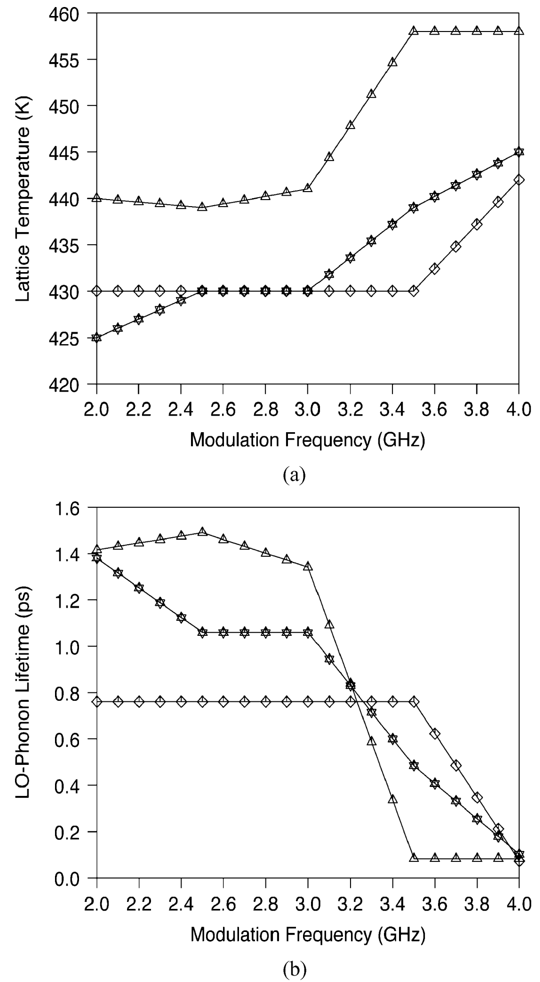

Fig. 5. Estimated variations of (a) lattice temperature, and (b) longitudinal optical phonon lifetime with modulation frequency. Triangle: $I_{\mathrm{dc}} = 18$ mA, star: $I_{\mathrm{dc}} = 20$ mA, and diamond: $I_{\mathrm{dc}} = 22$ mA.

(b), respectively. The values at other modulation frequencies were then obtained by interpolation. The explanation for these irregular characteristics is given in the final part of this analysis. As can be seen from the bifurcation maps shown in Fig. 6, the simulated result at a bias current of 18 mA does bear some resemblance to the measured result. However, the experimentally observed period-tripling, period-quadrupling, higher order bifurcation, and chaos at a bias current of 20 mA were not produced in the simulation. Similarly, simulation did not show the period-quadrupling behavior observed in measurement when the bias current was set at 22 mA. These missing details are due to the fact that the value of τ_ϵ was fixed, and a constraint was set on the lowest value of τ_{LO} to compromise for computational efficiency. In the next part of this investigation, the one-level carrier heating model was revisited taking into account the varying nature of T_L, and hence τ_ϵ as well.

As the constraint imposed on τ_{LO}, due to reasons of computational efficiency, was hindering the investigation of the effect of varying T_L on simulated behavior of LDs, the one-level carrier heating model in the final part of this analysis (where there is only one time constant in describing the decaying rate of the excess energy of carriers) was revisited with varying T_L and τ_ϵ taken into consideration. First of all, the best choice of T_L and τ_ϵ at each of the selected modulation frequencies over the frequency range from 2.0 to 4.0 GHz was acquired using the previously described method. The resulting graphs of T_L and τ_ϵ versus the modulation frequency are shown in Fig. 7(a) and (b), respectively. With these values of T_L and τ_ϵ, the simulated bifurcation maps (Fig. 8) showed good agreement with measured results [14]. The observed discrepency at a bias current of 18 mA for modulation currents and frequencies ranging from 18 to 22 mA and 2.6 to 2.8 GHz, respectively, is attributed

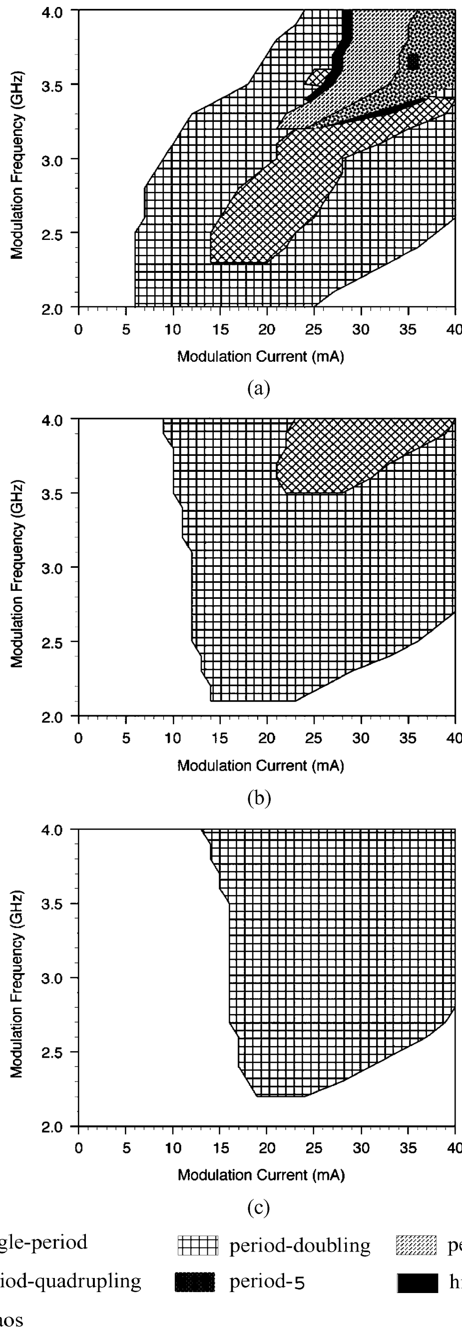

Fig. 6. Regions of simulated bifurcation. (a) $I_{\mathrm{dc}} = 18$ mA. (b) $I_{\mathrm{dc}} = 20$ mA. (c) $I_{\mathrm{dc}} = 22$ mA.

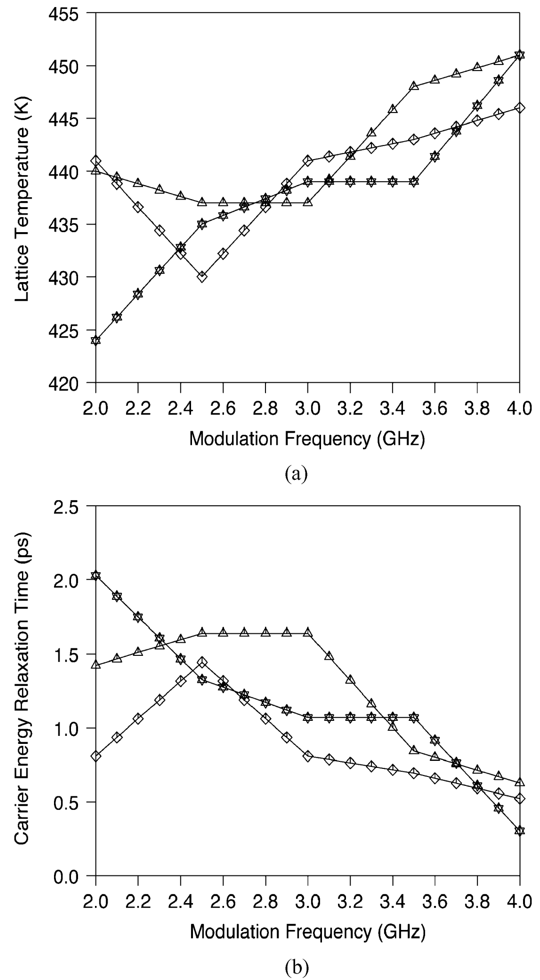

Fig. 7. Graphs of (a) Lattice temperature. (b) τ_ϵ versus modulation frequency. The effects of bandgap shrinkage and carrier-induced index change were taken into account in the simulations. Triangle: $I_{\mathrm{dc}} = 18$ mA, star: $I_{\mathrm{dc}} = 20$ mA, and diamond: $I_{\mathrm{dc}} = 22$ mA.

to the fact that the dependence of τ_ϵ on modulation current has not been considered exclusively. Even so, simulations still yield remarkable agreement with measured results. The phenomena that gave rise to the characteristics of the T_L and τ_ϵ versus modulation frequency graphs shown in Fig. 7(a) and (b), respectively, are explained as follows. Due to nonlinearity and the parasitic capacitance of LDs, the number of carriers injected into the active layer under large-signal conditions differs from one modulation frequency to another. Therefore, at different modulation currents and frequencies, the carrier energy is different, which results in irregular characteristics of carrier energy relaxation time as a function of bias current [Fig. 7(b)]. However, for simplicity, the dependence of carrier energy relaxation time on the modulation current has not been exclusively considered here. The dependence of lattice temperature on bias current is directly related to that of the carrier energy relaxation time, because the temperature transfer rate from carriers to the lattice is determined by the carrier energy relaxation time. Therefore, the lattice temperature rises as the carrier energy relaxation time decreases, which explains the result shown in Fig. 7(a). However, the generally increasing trend of the lattice temperature as the modulation frequency increases seems questionable. Nevertheless, this can be explained as follows. Clearly, as the modulation frequency increases, a larger portion of the modulation current will bypass the active layer and flow through the shunt capacitance of the LD current blocking layers to the ground. This means that the average energy of the carriers within the active layer is lower [in agreement with Fig. 7(b)], hence the lattice temperature should also decrease instead of rising [Fig. 7(a)]. However, in reality, resistive heating also contributes to the lattice temperature. When the modulation

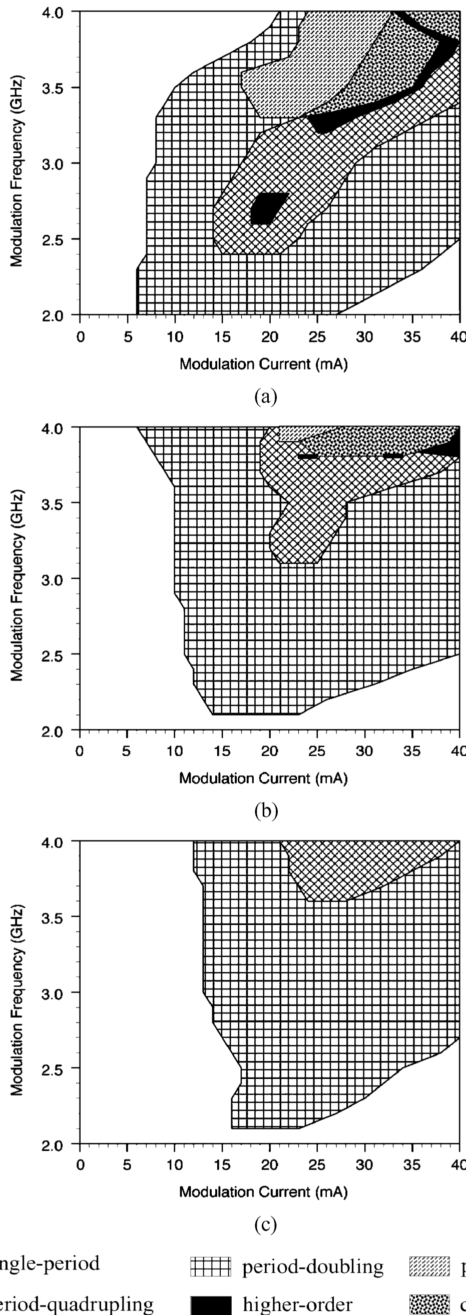

Fig. 8. Regions of bifurcations. (a) $I_{\rm dc} = 18$ mA. (b) $I_{\rm dc} = 20$ mA. (c) $I_{\rm dc} = 22$ mA. Calculated using one-level carrier heating model with varying lattice temperature, bandgap shrinkage effect, and carrier-induced index change.

frequency increases, the conversion efficiency of the laser diode drops, and a larger portion of the modulation current is shunted to the ground. This explains the generally rising lattice temperature as the modulation frequency increases [Fig. 7(a)]. Hence, although the temperature contribution from Joule heating might be relatively much smaller compared to other temperature contribution processes [25], it might have some influence as far as further improvement of simulation accuracy is concerned, especially for the situation where the LD is subjected to large signal high-frequency modulation.

IV. Conclusion

For the first time, a carrier heating model has been used to study the nonlinear dynamics of LDs. Simulations performed on a 1.55-μm DFB LD revealed the importance of taking bandgap shrinkage into account. Carrier-induced index change, and hence wavelength drift, was found to have negligible effect on the calculated nonlinear behavior of LDs. Simulations that account for the varying nature of lattice temperature and carrier energy relaxation time supports the current-dependent gain suppression concept proposed in [21], [22]. Further analysis suggested that the lattice temperature variation could be due to resistive heating. Hence, it is postulated here that in order to accurately reproduce the measured nonlinear behavior of LDs in simulations, resistive heating might have to be accounted for.

References

[1] C. H. Lee, T. H. Yoon, and S. Y. Shin, "Period doubling and chaos in a directly modulated laser diode," *Appl. Phys. Lett.*, vol. 46, pp. 95–97, Jan. 1985.

[2] K. Y. Lau and A. Yariv, "Ultra-high speed semiconductor lasers," *IEEE J. Quantum Electron.*, vol. QE-21, no. 2, pp. 121–138, Feb. 1985.

[3] Y. C. Chen, H. G. Winful, and J. M. Liu, "Subharmonic bifurcations and irregular pulsing behaviour of modulated semiconductor lasers," *Appl. Phys. Lett.*, vol. 47, pp. 208–210, Aug. 1985.

[4] M. Tang and S. Wang, "Simulation studies of bifurcation and chaos in semiconductor lasers," *Appl. Phys. Lett.*, vol. 48, pp. 900–902, Apr. 1986.

[5] M. Tang and S. Wang, "Simulation studies of the dynamic behaviour of semiconductor lasers with Auger recombination," *Appl. Phys. Lett.*, vol. 50, pp. 1861–1863, Jun. 1987.

[6] Y. Hori, H. Serizawa, and H. Sato, "Chaos in a directly modulated semiconductor laser," *J. Opt. Soc. Amer. B.*, vol. 5, pp. 1128–1132, May 1988.

[7] Y. G. Zhao, "Simulation studies of frequency locking, quasi-periodicity, subharmonic bifurcation, and chaos in modulated semiconductor lasers," *IEEE J. Quantum Electron.*, vol. 28, no. 10, pp. 2009–2015, Oct. 1992.

[8] R. S. Tucker and I. P. Kaminow, "High-frequency characteristics of directly modulated InGaAsP ridge waveguide and buried heterostructure lasers," *IEEE J. Lightw. Technol.*, vol. LT-2, no. 8, pp. 385–393, Aug. 1984.

[9] R. S. Tucker, "High-speed modulation of semiconductor lasers," *IEEE J. Lightw. Technol.*, vol. LT-3, no. 12, pp. 1180–1192, Dec. 1985.

[10] N. H. Jensen, P. L. Christiansen, and O. Skovgaard, "On period doubling bifurcations in semiconductor lasers," *Proc. Inst. Elect. Eng.—Optoelectron.*, vol. 135, pp. 285–288, Aug. 1988.

[11] L. Chusseau, E. Hemery, and J.-M. Lourtioz, "Period doubling in directly modulated InGaAsP semiconductor lasers," *Appl. Phys. Lett.*, vol. 55, pp. 822–824, Aug. 1989.

[12] T. Y. Yoon, C. H. Lee, and S. Y. Shin, "Perturbation analysis of bistability and period doubling bifurcations in directly-modulated laser diodes," *IEEE J. Quantum Electron.*, vol. 25, no. 9, pp. 1993–2000, Sep. 1989.

[13] E. Hemery, L. Chusseau, and J. M. Lourtioz, "Dynamics behaviours of semiconductor lasers under strong sinusoidal current modulation: modeling and expermient at 1.3 μm," *IEEE J. Quantum Electron.*, vol. 26, no. 4, pp. 633–641, Apr. 1990.

[14] H. F. Liu and W. F. Ngai, "Nonlinear dynamics of a directly modulated 1.55 μm InGaAsP distributed feedback semiconductor laser," *IEEE J. Quantum Electron.*, vol. 29, no. 6, pp. 1668–1674, Jun. 1993.

[15] S. Bennett, C. M. Snowden, and S. Iezekiel, "Nonlinear dynamics in directly modulated multiple-quantum-well laser diode," *IEEE J. Quantum Electron.*, vol. 33, no. 11, pp. 2076–2083, Nov. 1997.

[16] H. Lamela, G. Carpintero, and F. J. Mancebo, "Period tripling and chaos in the dynamic behavior of directly modulated diode lasers," *IEEE J. Quantum Electron.*, vol. 34, no. 10, pp. 1797–1801, Oct. 1998.

[17] S. F. Yu, "Nonlinear dynamics of vertical-cavity surface-emitting lasers," *IEEE J. Quantum Electron.*, vol. 35, no. 3, pp. 332–341, Mar. 1999.

[18] J. Manning, R. Olshansky, D. M. Fye, and W. Powazinik, "Strong influence of nonlinear gain on spectral and dynamic characteristics of InGaAsP lasers," *Electron. Lett.*, vol. 21, pp. 496–497, May 1985.

[19] G. P. Agrawal, "Effects of nonlinear gain on single-frequency behaviour of semiconductor lasers," *Electron. Lett.*, vol. 22, pp. 696–697, Jun. 1986.

[20] G. P. Agrawal, "Effects of gain nonlinearities on period doubling and chaos in directly modulated semiconductor lasers," *Appl. Phys. Lett.*, vol. 49, pp. 1013–1015, Oct. 1986.

[21] C. G. Lim, S. Iezekiel, and C. M. Snowden, "Is noise a crucial factor in rate equation modelling of nonlinear dynamics in laser diodes?," *Appl. Phys. Lett.*, vol. 77, pp. 3493–3495, Nov. 2000.

[22] C. G. Lim, S. Iezekiel, and C. M. Snowden, "Influence of the injection current dependence of gain suppression on the nonlinear dynamics of semiconductor lasers," *Appl. Phys. Lett.*, vol. 78, pp. 2384–2386, Apr. 2001.

[23] S. Schuster and H. Haug, "Calculation of the gain saturation in CW semiconductor lasers with Boltzmann kinetics for Coulomb and LO phonon scattering," *Semicond. Sci. Technol.*, vol. 10, pp. 281–289, Mar. 1995.

[24] Z. Toffano and A. Destrez, "New gain compression factor determination by harmonic analysis in semiconductor lasers," *Electron. Lett.*, vol. 31, pp. 202–203, Feb. 1995.

[25] R. Ait-Sadi, A. J. Lowery, and B. Tuck, "Two-dimensional temperature modelling of DH laser diodes using the transmission-line modelling (TLM) method," *Proc. Inst. Elect. Eng.—Sci. Meas. Technol.*, vol. 141, pp. 7–14, Jan. 1994.

[26] M. Szymanski, M. Zbroszczyk, and B. Mroziewicz, "The influence of different heat sources on temperature distributions in broad-area diode lasers," *Proc. Conf. Advanced Optoelectronics and Lasers*, Alushta, Crimea, Ukraine, vol. 1, pp. 252–254, Sep. 2003.

[27] L. V. Asryan, N. A. Gun'ko, A. S. Polkovnikov, R. A. Suris, G. G. Zegrya, B. B. Elenkrig, S. Smetona, J. G. Simmons, P. K. Lau, and T. Makino, "High-power and high-temperature operation of InGaAsP/InP multiple quantum well lasers," *Semicond. Sci. Technol.*, vol. 14, pp. 1069–1075, 1999.

[28] N. K. Dutta and R. J. Nelson, "Gain measurements in 1.3 μm InGaAsP-InP double heterostructure lasers," *IEEE J. Quantum Electron.*, vol. QE-18, no. 1, pp. 44–48, Jan. 1982.

[29] V. B. Gorfinkel and S. Luryi, "Fundamental limits for linearity of CATV lasers," *IEEE J. Lightw. Technol.*, vol. 13, no. 2, pp. 252–259, Feb. 1995.

[30] L. D. Westbrook, "Measurements of dg/dN and dn/dN and their dependence on photon energy in $\lambda = 1.5$ μm InGaAsP laser diodes," *Proc. Inst. Elect. Eng.—Optoelectron.*, vol. 133, pp. 135–142, Apr. 1986.

[31] G. P. Agrawal and N. K. Dutta, *Semiconductor Lasers*, 2nd ed. New York: Van Nostrand, 1993.

[32] C. G. Lim, "Rate equation modelling of nonlinear dynamics in directly modulated and self-pulsating semiconductor lasers," Ph.D. dissertation Dept. Electron. Elect. Eng., Inst. Microwave and Photonics, Univ. Leeds, Leeds, U.K., 2001.

[33] K. L. Hall, G. Lenz, E. P. Ippen, U. Koren, and G. Raybon, "Carrier heating and spectral hole burning in strained-layer quantum-well laser ampifiers at 1.5 μm," *Appl. Phys. Lett.*, vol. 61, pp. 2512–2514, Nov. 1992.

Cheng Guan Lim (S'94–A'97–M'00) was born in Singapore in 1971. He received the B. Eng. (Honours) degree in electronic and electrical engineering in 1997 and the Ph.D. degree at the Institute of Microwave and Photonics of Department of Electronic and Electrical Engineering from the University of Leeds, Leeds, U.K., in 2001.

From 2001 to 2003, he was a Research Engineer at the Yokohama Research and Development Laboratories of The Furukawa Electric Company, Yokohama, Japan, working on the development of semiconductor laser modules for digital and analog telecommunication applications. In 2003, he joined Agilent Technologies, Singapore, as a Senior Engineer focusing on optoelectronic device manufacturing. From 2004 to 2005, he was a Senior Research Scientist at the Institute for Infocomm Research, Singapore, (a member of the Agency for Science, Technology and Research-Singapore, and a National University of Singapore affiliated research institute) dealing with radio-over-fiber technologies. Presently, he is an Assistant Professor at the Department of Photonics/Institute of Electro-Optical Engineering, National Chiao Tung University, Hsinchu, Taiwan R.O.C. where he is establishing the Computational Optoelectronics and Optical-components Laboratory (COOL). His prime research interest is in semiconductor device physics, in particular high-speed semiconductor devices used in communication systems, modelling and simulation of advanced semiconductor devices. At present, he is especially interested in optical injection technique for performance enhancement in radio-over-fiber systems; optical generation and modulation of microwave/millimeter-waves based on optical injection phase-locked loop; developing a quick CSO and CTB evaluation scheme for CATV laser diodes; and photonic integrated circuits (PICs). He has one pending U.S. patent, one pending Japanese patent, and published several international refereed journal and conference papers.

Dr. Lim has served as a Steering Committee Member for the Inaugural IEEE International Workshop on Antenna Technology 2005 (Singapore), and as a Technical Program Committee member for the 2005 Symposium on Technology Fusion of Optoelectronics and Communications-International Conference on Photonics. In 1995, he was awarded the Crab Tree Prize for outstanding academic achievement, the Hewlett-Packard Prize in 1997 for the recognition as the best student in high-frequency engineering, and the F. W. Carter Prize in 2001 for presenting the best Ph.D. thesis.

Stavros Iezekiel (S'88–M'90–SM'00) received the B.Eng. and Ph.D. degrees in electronic and electrical engineering from the University of Leeds, Leeds, U.K., in 1987 and 1991, respectively. His Ph.D. studies concerned the nonlinear dynamics of laser diodes.

From 1991 to 1993, he worked in conjunction with M/A-COM Corporate R&D Center on the development of microwave photonic multichip modules. He is now a Senior Lecturer at the University of Leeds, where he leads the research activity in microwave photonics.

Dr. Iezekiel received the 1999 IEE Measurement Prize for his work on lightwave network analysis. As a member of the UKRI MTT/ED/AP/LEO Joint Chapter AdCom, he has organized a number of IEEE events, and he is also the U.K. Representative for Commision D of URSI.

Christopher M. Snowden (S'82–M'82–SM'91–F'96) received the B.Sc. (Hons.), M.Sc., and Ph.D. degrees in electronic and electrical engineering from the University of Leeds, Leeds, U.K., in 1977, 1979, and 1982, respectively.

He is Vice-Chancellor and Chief Executive of the University of Surrey, Surrey, U.K. Prior to this, he was Chief Executive Officer of Filtronic ICS. He joined Filtronic plc in 1998 as Director of Technology before being promoted to Joint Chief Executive Officer in 1999. He is a non-executive Director of Intense Ltd., designing and manufacturing photonic products, and CENAMPS Ltd., which is involved in microsystems and nanotechnology. He is a member of the U.K.s National Advisory Committee on Electronic Materials and Devices, and an Advisor on the U.K.s Office of Science and Technology/DTI Foresight Programme. He is Deputy Chairman of the European Microwave Association. He worked as the Senior Staff Scientist in Corporate Research and Development at M/A-COM Inc. in the USA, from 1989 to 1991. He has been a consultant for several other major international microwave electronics companies in the USA and U.K. He held the personal Chair of Microwave Engineering at the University of Leeds from 1992 to 2005 and during the period 1995–98 he was Head of the School of Electronic and Electrical Engineering. He was the Founder and first Director of the Institute of Microwaves and Photonics located in the School. During his time at Leeds, he has supervised 49 successful Ph.D. candidates. He was a Visiting Professor at the University of Durham until 2005.

Prof. Snowden is a Fellow of the Royal Academy of Engineering, a Fellow of the IEE, and a Fellow of the City and Guilds Institute. He was awarded the Royal Academy of Engineering's Silver Medal in 2004. He is currently a Distinguished Lecturer for the IEEE Electron Devices Society. He was awarded the 1999 Microwave Prize of the IEEE Microwave Theory and Techniques Society. He has written eight books and over 300 papers. He is a member of the IEEE Compound Semiconductor Device Technology Committee.